Journal of Power Sources 249 (2014) 92–102

Contents lists available at ScienceDirect

Journal of Power Sources

journal homepage: www.elsevier.com/locate/jpowsour

State of charge estimation of high power lithium iron phosphate cells

T. Huria, G. Ludovici, G. Lutzemberger*

Department of Energy, Systems, Territory and Constructions Engineering, University of Pisa, Largo Lucio Lazzarino n. 1, 56123 Pisa, Italy

HIGHLIGHTS

- The difficulties for SOC evaluation of the LFP cell were analysed.
- An algorithm for SOC evaluation has been developed.
- The modelling of the voltage hysteresis was introduced.
- Treatment of measurements errors was done using a Kalman filter.
- The algorithm effectiveness has been evaluated through measurements taken from lab tests.

ARTICLE INFO

Article history:
Received 15 July 2013
Received in revised form
14 October 2013
Accepted 17 October 2013
Available online 25 October 2013

Keywords:
Lithium battery
Battery modelling
State of charge evaluation
Extended Kalman filter
Electric vehicles
Hybrid vehicles

ABSTRACT

This paper describes a state of charge (SOC) evaluation algorithm for high power lithium iron phosphate cells characterized by voltage hysteresis. The algorithm is based on evaluating the parameters of an equivalent electric circuit model of the cell and then using a hybrid technique with adequate treatment of errors, through an additional extended Kalman filter (EKF). The model algorithm has been validated in terms of effectiveness and robustness by several experimental tests.

1. Introduction

The lithium iron phosphate (LFP) has emerged as one of the favoured cathode materials for lithium ion batteries, especially for use as an energy storage device (ESS) in hybrid electric vehicles (HEV) and electric vehicles (EV), thanks to its high intrinsic safety, capacity for fast charging and long cycle life [1]. Recent research and development in this technology, especially the introduction of the *nanoscale* LFP cells has led to phenomenal increases in its specific energy. Their voltage balance of 3.3 V per cell is also ideal for new applications such as lithium ion starting-lighting-ignition (SLI) batteries [2]. Graphite is used a as negative electrode. These cells have entered series production and are being marketed as custom *off-the-shelf* solutions for the emerging HEV and EV market by a number of companies today. The commercially available high-power *nanoscale* LFP cells can deliver and accept 30–35 times their normal current rates, and match the performance of the latest super-capacitors over short time periods.

The most important metric for an electrochemical ESS such as a rechargeable lithium battery is the accurate runtime evaluation of its state of charge (SOC), which is defined as the percentage of the completely extractable charge capacity remaining in the battery. The SOC indicates the amount of electrical energy remaining in the battery pack. An accurate runtime estimate of the SOC is important both for the battery application designers as well as for the battery users. Armed with the insight that the battery SOC would be determined accurately, the designer is able to efficiently use available battery capacity and ensures less designed-redundancy in its capacity; thus providing for smaller and lighter batteries. With

List of acronyms: EKF, Extended Kalman filter; ESS, energy storage system; EV, electric vehicle; HEV, hybrid electric vehicle; LFP, lithium iron phosphate; MST, Multiple Step Test; OCV, open circuit voltage; SLI, starting lighting ignition; SOC, state of charge.

* Corresponding author. Tel.: +39 050 2217384.
E-mail address: lutzemberger@dsea.unipi.it (G. Lutzemberger).

0378-7753/$ – see front matter © 2013 Elsevier B.V. All rights reserved.
http://dx.doi.org/10.1016/j.jpowsour.2013.10.079

an accurate indication of the battery SOC, the user ensures that the battery is not over-charged or under-discharged; and suffers less *range anxiety*. Overall, the battery lasts longer and provides a better performance.

Over the years, many techniques have been proposed for estimation of the battery SOC, which depend upon the battery chemistry and the final application [3,4]. The most reliable test for establishing the SOC of a battery is to charge or discharge it completely, thus physically reaching 100% or 0% SOC. This is often adopted for an EV or a *plug-in* HEV that are charged completely every evening, and allows the onboard SOC estimation algorithm to gain valuable feedback from this activity to recalibrate itself. However, for a usual HEV that is never charged from the grid, ampere hour counting (also called the book-keeping system), which uses the value of the current integral as a direct indicator of SOC, remains the most popular technique. Since the integration of current offsets or uncompensated and systematic effects can increase the uncertainty of measurements, a periodical correction of this technique, using correction point, is required.

The open circuit voltage (OCV) vs SOC correlation curve is often used to provide correction points for the recalibration, but it cannot be used by alone for batteries that exhibit hysteresis and have a very flat OCV–SOC correlation curve, such as for LFP batteries. Moreover these batteries have capabilities similar to the supercapacitors: thus they can be able to deliver very high current for very short time periods (almost 35 times their nominal value). For this reason small changes of the offset or the effects mentioned above could produce an integration drift. Hence, it is necessary to develop a robust algorithm able to accurately estimate the instantaneous charge stored in the battery with the characteristics described above. Different techniques have been adopted in the past to estimate the battery SOC, combining them with hysteresis estimation models [5–7], especially using the Extended Kalman filter [8–11].

This paper presents a technique to estimate the SOC of an LFP battery, that is able to replicate the hysteresis behaviour of the OCV–SOC correlation curve, using a simple equivalent circuit model presented in Ref. [12] with the addition of an extended Kalman filter to reduce the measurements uncertainty. Section 2 presents the challenges for SOC evaluation applied to LFP batteries, Section 3 explains the algorithm model definition and Section 4 the application of the method to several different case studies.

2. Challenges

2.1. Voltage relaxation time

As mentioned in the Introduction, the OCV–SOC correlation curve is often used to correct the current integral errors during runtime. This is usually done when the vehicle has been at rest (with its battery neither charging nor discharging) for a long time (30 min–1 h), and when its battery voltage at the terminals is assumed to approximate the value of the OCV. This assumption is valid for most of the battery chemistries. An attempt was made to validate this assumption for the nanoscale LFP cells using pulse discharge and charge tests. Under this test, the cell was first completely charged, rested for 2 h and then subjected to ten discharge pulses interspersed by 1 h rest phases till the cell was completely discharged. Subsequently, the cell was charged using ten charge pulses interspersed by 1 h rest phases till the cell was completely charged. The cell was then allowed to rest for 13 h Fig. 1 presents the plot of the cell terminal current and voltage measurements during the complete pulse discharge and charge experimental test.

The primary interest in the experiment was in validating the assumption that the voltage of the nanoscale LFP cell relaxes to approximately reach its OCV after a long rest of 1 h. However, it was observed that after the complete pulse discharge and charge test (Fig. 1), when the SOC reached 100%, the voltage did not relax to its OCV even after 13 h. However, it was found that the voltage relaxation time was considerably less between the 30–70% SOC window (time constant of around 800 s), compared to when the SOC was near 0% or 100%.

Additionally, as seen from the characteristics of the nanoscale LFP cell by a prominent manufacturer presented in Table 1, the cell has a current capability of over 35 times its nominal current capacity; thus, even the offsets in the current measurement would integrate (in the current integral SOC evaluation technique) very rapidly, to reach a significant fraction of the total cell capacity in a small time period. Thus, for an accurate runtime estimation of the SOC of these cells, the current integral SOC evaluation technique would need to be corrected using the OCV–SOC correlation curve much more frequently (at most every one or 2 h) as compared to after eight to 10 h of operation for other battery chemistries. This is another significant challenge to be overcome.

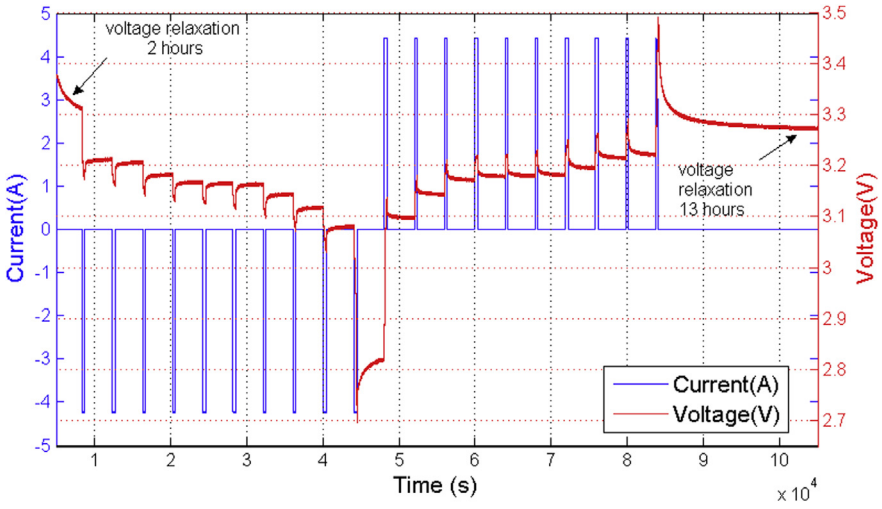

Fig. 1. Current and voltage plots with time for Multiple Step Test.

Table 1
Test LFP cell specification.

Characteristic	Value
Cell capacity (minimum)	4.4 Ah
Cell voltage (nominal)	3.3 V
Energy content (nominal)	14.5 Wh
Discharge power (nominal)	550 W
Operating temperature	−30 °C to 55 °C
Storage temperature	−40 °C to 60 °C

2.2. Hysteresis and flat OCV–SOC correlation

As inferred from the pulse discharge and charge experimental test (Fig. 1), the voltage at rest was plotted with respect to the SOC for different times of rest, to estimate the marked hysteresis the nanoscale LFP cells exhibit. In fact, the hysteresis is correlated with the long voltage relaxation time, with the level of hysteresis decreasing with the rest period, as visible in Fig. 2.

This shows that the nature of the hysteresis is not steady but changes with time. Furthermore, the pulse discharge and charge tests also produced the OCV–SOC correlation curve for the cell as shown in Fig. 3. It is apparent that in the SOC window of 40%–60% the curve is extremely flat. Moreover, for the entire length of the SOC window from 20% to 80%, the voltage gradient is of the order of 0.1 V. Even a small error in voltage measurement, would lead to extremely inaccurate results. Thus, implementing the usual algorithm of using an OCV–SOC correlation curve to correct the integral current to estimate the SOC of the battery at runtime is a challenge.

2.3. Low temperature performance

The performance of LFP cells have been reported in literature to be adversely affected by low ambient temperatures [13–16]. Preliminary tests at different temperatures were designed to verify the ability of the cell to deliver and accept current at a required value. As seen from Fig. 4, the test was successful at 20 °C. At 0 °C, the cell demonstrated the required discharge capability, but was unable to charge as the cell voltage breached the upper limit of 3.6 V. Both at −15 °C and −20 °C, the cell was unable to deliver the required power in both discharge and charge.

It is to be noted that during charge at −15 °C and −20 °C the current did not reach the imposed required value, because of the voltage limitation. The charging hardware automatically limited the charge current to avoid cell damage; the charging phase is not immediately stopped so that the shapes show what happens. The delay between reaching of cell voltage limitation and actual stopping of the current is around half a second. Thus, the difficulty encountered in the *nanoscale* LFP cell tested was its inability to deliver or accept more than 20% of the power specified by the manufacturer, especially at temperatures below 0 °C. These aspects require the presence of a battery package thermostatically controlled, to be continuously maintained at the reference temperature of 20 °C. The battery model was developed taking into account this operating condition.

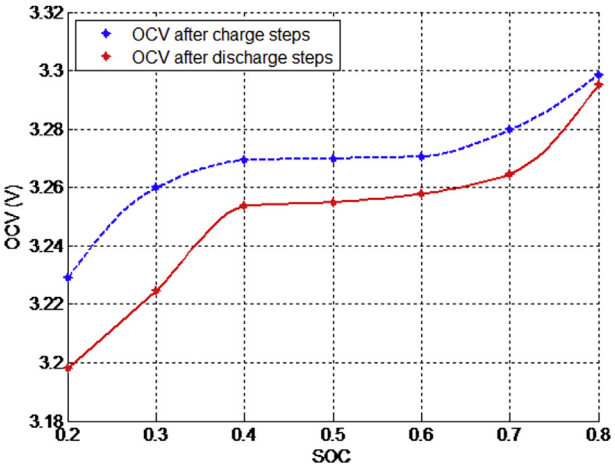

Fig. 3. Flat OCV–SOC correlation curve for nanoscale LFP cells.

3. Algorithm formulation

3.1. The battery model

A typical mathematical model for modelling electrochemical cells was shown in Fig. 5. The two representations are substantially equivalent, where I_t is the *terminal current*, i.e. the current that enters the cell terminals, and I_m is the *main current*, i.e. the current that determines the charge storage.

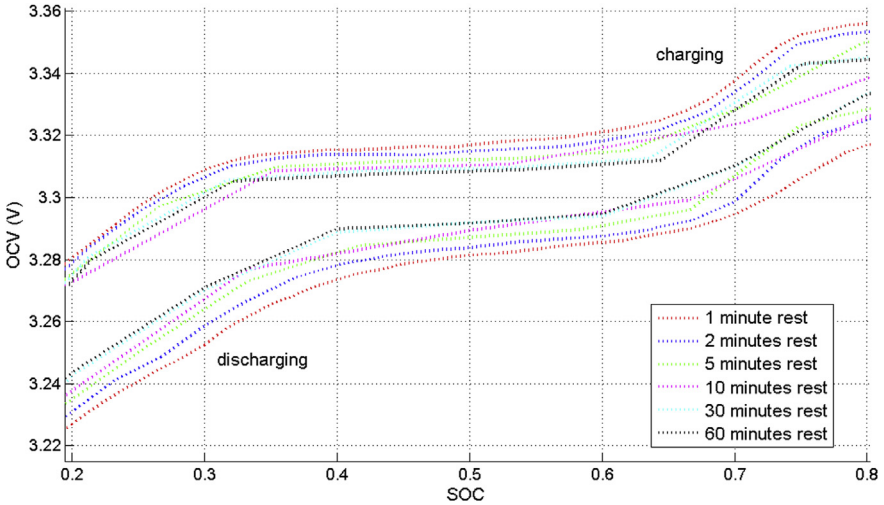

Fig. 2. Hysteresis decreasing with rest between pulses in the Multiple Step Test on LFP cell (20 °C).

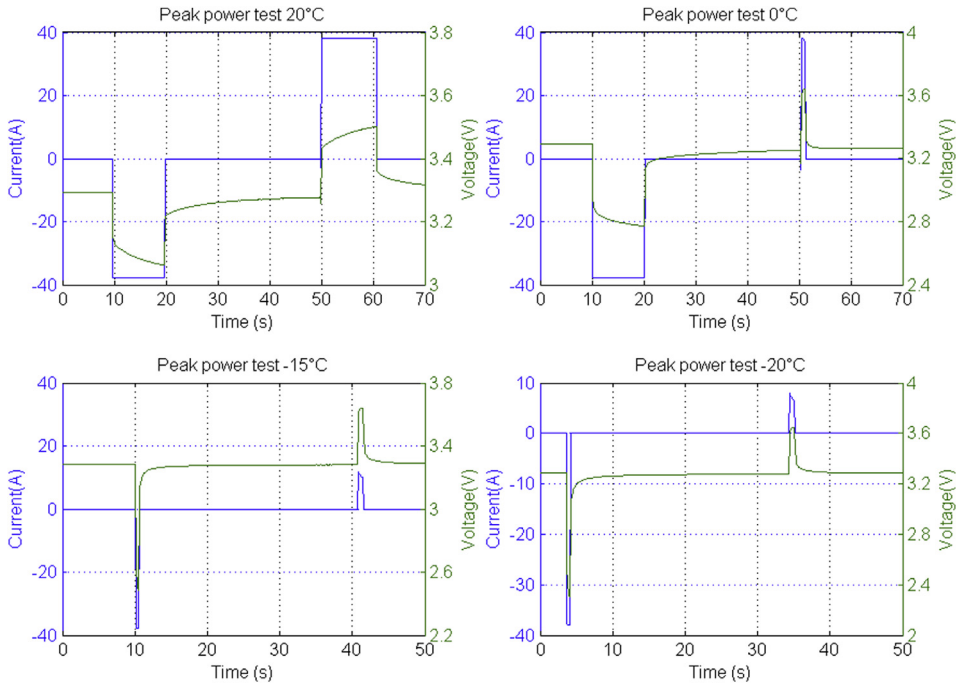

Fig. 4. Results of the peak power test at different temperatures.

The left part of the lower circuit is a fiction electric network, the capacitance and resistance are not dimensionally equivalent to the real ones. U_{SOC} is a dimensionless voltage between 0 and 1 numerically equal to the cell's SOC itself, while U_{OC} is the OCV of the cell that is a function of the cell SOC. The SOC of the cell can be defined as follows:

$$\mathrm{SOC}(t) = \mathrm{SOC}(0) + \frac{1}{C_Q}\int_0^t i_m(t)\mathrm{d}t \tag{1}$$

where C_Q is the capacity of the battery cell ($C_Q = 3600C_{nom}$). The transient behaviour of the cell is modelled by the network of resistances (R_0, R_1 and R_2) and the capacitors (C_1 and C_2) as described in the set of equation (2).

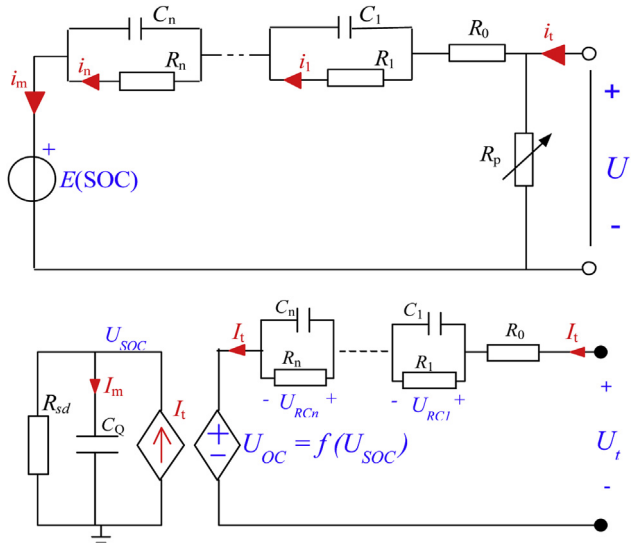

Fig. 5. Equivalent circuit models adopted for electrochemical cells.

$$\begin{cases} \dot{U}_{SOC} = -\frac{U_{SOC}}{R_{sd}C_q} + \frac{I_t}{C_q} \\ \dot{U}_{RC_1} = -\frac{U_{RC_1}}{R_1C_1} + \frac{I_t}{C_1} \\ \dot{U}_{RC_2} = -\frac{U_{RC_2}}{R_2C_2} + \frac{I_t}{C_2} \\ U_t = U_{OC} + R_0I_t + U_{RC_1} + U_{RC_2} \end{cases} \tag{2}$$

Additionally, it has also to be noted that:

- The parasitic non-linear resistor R_p, simulates all phenomena that yield coulombic efficiency lower then unity for the cell, including self-discharge.
- The resistor R_{sd}, simulates the effects of self-discharge.

The effects of R_p and R_{sd} can be normally neglected when analysing short time tests and can be observed only when considering very long time-span, since they are related to parasitic effects, which for lithium batteries are very slow. Indeed it is known that if the tests are made lasting short times (not more than a few hours) the coulombic efficiency for this type off cell is near the unity.

Finally, the model does not include any hysteresis effect: the numerical values of voltage sources, resistances, capacitances are intended to be function of SOC and temperature, but not on the current direction.

In this paper SOC estimation is based on an equivalent circuit model with generic number of RC blocks, presented at the bottom of Fig. 5, that need to be chosen. Further details have been explained in next section.

3.2. Parameters identification

The identification of the parameters R_0, R_1, R_2, C_1, C_2 is based on the experimental Multiple Step Test (Fig. 1), that simulates the dynamic behaviour of the cell at different SOC at constant temperature (20 °C). Using equation (2), electrical parameters are

found by minimizing the error between actual and simulated voltage profile. The error function chosen is of the type:

$$\varepsilon = \sqrt{(U_{\text{actual}} - U_{\text{model}})^2} \tag{3}$$

The Multiple Step Test (MST) was performed in two flavours: charge-based and discharge-based. These two can be used to determine all the parameters of the cell's equivalent circuit, and the obtained values can be compared so as to verify differences in cell's behaviour when charging and discharging.

As already mentioned, the mathematical model has a generic number of R–C blocks, and the best value for n had to be chosen. The decision to determine the optimum number of R–C blocks was made between the two options $n = 1$ and $n = 2$, which avoided excessive complexity of the model and therefore of the procedure to evaluate the numerical values of parameters. To understand the process, the results obtained at the SOC = 50% are reported in Fig. 6, which shows a comparison between experimental and simulated voltage for $n = 1$ and $n = 2$ at the end of a discharge pulse.

The comparison shows that both models present rather acceptable results, while the 2-block one has a distinct advantage. As inferred from the green-curve, in comparison to the centre of the blue experimental band, the single block model presents a final value that is markedly lower than the actual OCV. Since the value of U_{OC} is very important for further analysis and algorithms for SOC estimation, it is advisable to force this number the most reasonable, as observable in the experimental data: this implies that the minimization of error between experimental and model trends is made acting just on R's and C's, while U_{OC} is taken as being known in advance. With $n = 2$, on the contrary, there is no need to constraint U_{OC}, since the error-minimization algorithm automatically gives an acceptable value for this parameter. Moreover, the two R–C block model gives very good result even during the first part of the considered transient. It was therefore concluded that two R–C blocks are important to keep good quality of the model reproduction, therefore this assumption has been adopted. If instead the charge-based MST is considered, the result when SOC = 50% is shown in Fig. 7.

The corresponding numerical parameters, following the same unaltered identification procedure, present different values during charge and discharge. This duality, however, is a potential source of difficulties, arising when the cell is subjected to continuously varying currents. Indeed, if the model parameters suddenly switch from charge to discharge values whenever the current at cell's terminals changes its sign, it is not difficult to foresee, large mismatches between simulation and actual values: the basic idea, that is similar to what often found in literature [6], is therefore of adopting hysteresis only for U_{OC}, and using intermediate values for the other parameters. Several techniques have been tested, i.e. the arithmetic mean evaluation between numerical values obtainable separately during end-of-charge and end-of-discharge, or minimizing the global error considering both end-of-charge and end-of-discharge transients. From the results it was observed that the two techniques are rather equivalent. The actual evaluation of numerical parameter of the model can therefore be done in either way: the choice could be made considering only practical issues related to the automatic determination of the numerical values from experimental tests.

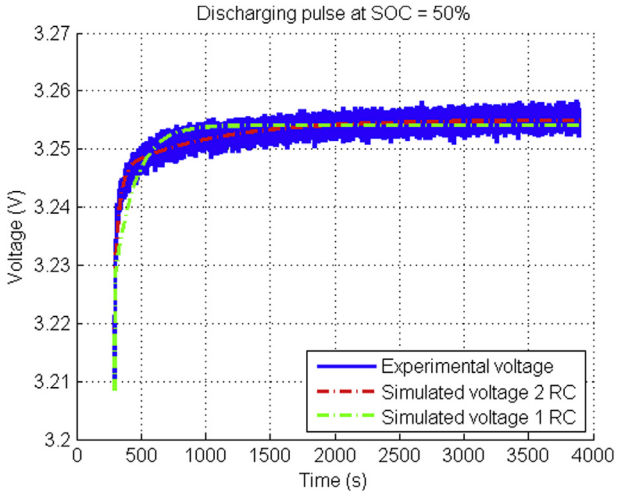

Fig. 6. Voltage behaviour at the end of the discharge process. Comparison between experiment and model.

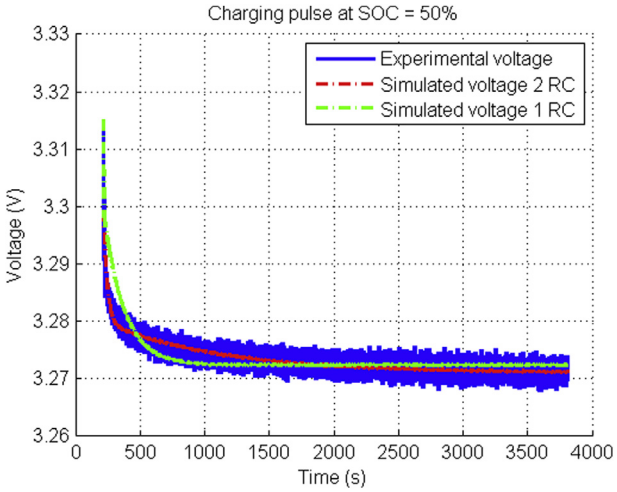

Fig. 7. Voltage behaviour at the end of the charge process. Comparison between experiment and model.

3.3. Hysteresis model

As Fig. 2 shows, the LFP cell exhibit hysteresis from 0 to 100% of SOC, therefore a mathematical model of the hysteresis behaviour of the cell has been developed [17]. The hysteresis model considers the cell electrical model (Fig. 5) as a dynamic system with respect to its SOC at all times; moreover it emulates the hysteresis in the OCV behaviour during both the major loops (0%–100% SOC) and the minor loop (small charge discharge cycle during a longer overall charge or discharge). Indeed, on-board hybrid vehicles in general, and HCV vehicle in particular, the SOC window during normal operation will be much smaller than the full potential SOC range.

The basic idea is to try to create a mathematical model that tends to move U_{OC} towards the upper curve when the cell is charging, and towards the lower one when it discharges. The speeds of this transition needs to be evaluated based on cell tests.

In pursuing this objective, after some attempts the following mathematical formulation has been proposed, that determines the derivative of U_{OC} as a function of the direction in which SOC is moving, and on how far actual model U_{OC} is from the target curve. The target curve is the upper curve (blue in web version in Fig. 8) when the cell is charging, the red one (in web version) when it is discharging.

$$\frac{dU_{OC}(U_{SOC})}{dU_{SOC}} = \begin{cases} \frac{dU_{OCch}(U_{SOC})}{dU_{SOC}} + k(U_{OCch}(U_{SOC}) - U_{OC}(U_{SOC})), & \frac{dU_{SOC}}{dt} \geq 0 \\ \frac{dU_{OCdisch}(U_{SOC})}{dU_{SOC}} + k(U_{OCdisch}(U_{SOC}) - U_{OC}(U_{SOC})), & \frac{dU_{SOC}}{dt} < 0 \end{cases} \quad (4)$$

The algorithm works as follows:

- when the time-derivative of U_{OC} is positive, the model U_{OC} is gradually moved towards U_{OCch}, (the blue curve in web version in Fig. 8) using a derivative that is the corresponding target derivative plus a correction factor.
- when the time-derivative of U_{OC} is negative, the model U_{OC} is gradually moved towards $U_{OCdisch}$, (the red curve in web version in Fig. 8) using a derivative that is the corresponding target derivative plus a correction factor.

Therefore, the dimensionless parameter k determines the speed of transition from one curve to the other, and therefore is called *transition speed* of the algorithm.

Some tests have been prepared which refers to the somewhat idealized voltage behaviour shown in Fig. 3. The algorithm has been tested submitting the algorithm (4) to a sinusoidal input SOC varied between two limits: for instance the result between SOC = 0.2 and SOC = 0.4, using a value of $k = 10$ is shown in Fig. 8.

This figure clearly shows that when SOC increases, the model U_{OC} (green curve in web version) tends to approach the upper U_{OC} bound (blue curve in web version), while when SOC decreases it tends to approach the lower bound (red curve in web version).

Several other tests have been performed to test the robustness of the algorithm, using more realistic SOC trends able to simulate the ordinary vehicle operation, in which a power contribution is also coming from the internal combustion engine, that vertically offsets the profile in such a way that the charge does not vary during vehicle operation (Fig. 9).

3.4. Algorithm SOC estimator

As discussed in the previous section, the difficulties of the most common ways to estimate cell's SOC are related to the Ampere-hour counting technique, or to the OCV–SOC correlation.

Ampere-hour counting normally creates accumulated errors that, for the high power cells, can reach 10% in as a small time as 20 min. Therefore this technique can be used only for very short times.

OCV–SOC correlation brings the difficulty that for the central SOC zone OCV is nearly horizontal, and that there is a marked hysteresis phenomenon that further complicates the analysis.

The basic idea that was issued is to cycle between ampere-hour counting and OCV estimation, to compensate the errors. The algorithm basic arrangement can therefore be as shown in Fig. 10.

The measures of the cell's voltage and current are taken from the physical system, as shown in the upper part of the figure. These two measures are fed into the Hybrid SOC evaluator, that then gives the output. The evaluator operates in two directions:

- In the upper chain it makes a voltage-based SOC evaluation: from the measured cell's terminal voltage U_t, determines the open-circuit U_{OC} (by subtraction of the voltage drop across the electric network R_0, R_1C_1, R_2C_2) and then, using the above discussed SOC–OCV correlation, estimates the *SOC_U*.
- In the block containing 1/(Cs) ("in which "s" is the Laplace variable) another SOC estimation is obtained, based on ampere-hour counting.

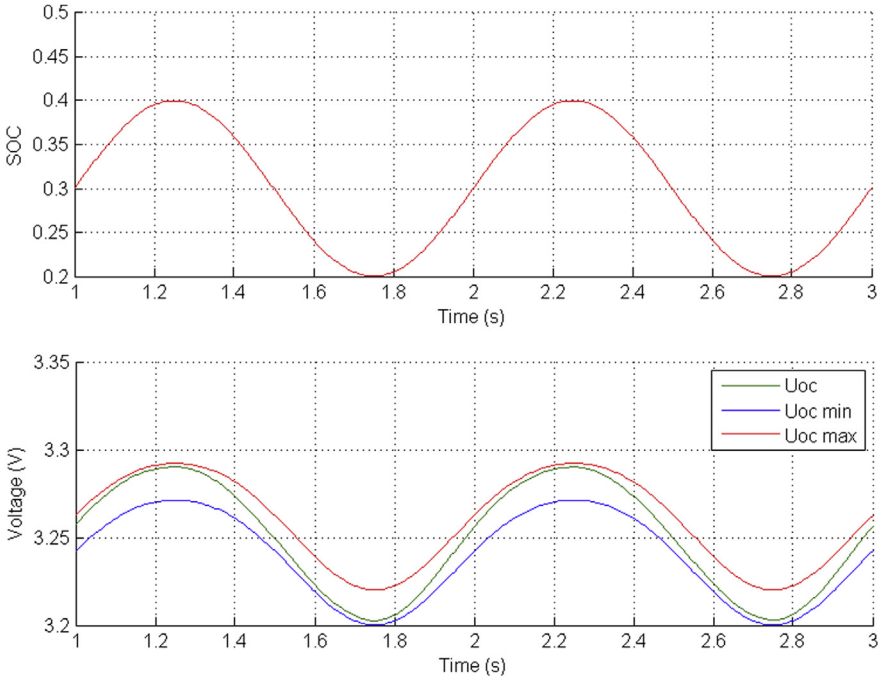

Fig. 8. Effect of the algorithm in a sample case.

The two SOC evaluations must then be somehow mixed to determine the final estimate *SOC_ev*. In addition to the technique depicted in Fig. 11, adequate treatment of measuring errors must be made, for instance by taking advantage of Kalman filters. After some attempts, the final implementation of the basic logic shown in Fig. 10, which showed a good estimation quality as represented in Fig. 11 (where the upper part of Fig. 10 is omitted for the sake of simplicity), was obtained.

In comparison to Fig. 10, the following differences have been introduced: instead of a simple hysteresis block, a full Extended Kalman filter has been introduced, that performs SOC evaluation taking also into account the measured current I_m, (Fig. 5) and adequately treating measurement errors.

The Extended Kalman Filter (EKF) is an optimum state estimator for nonlinear systems, where a linearization process is applied to the OCV–SOC correlation curve at each step, in order to approximate the nonlinear system as a linear time varying (LTV) system. The EKF is able to estimate the best possible values of the output based on input containing unmeasured noise.

The set of equation (2) describes the dynamic linear system represented in Fig. 5, reproducing the battery transient behaviour whose parameters are functions of the *SOC* and changing with time. Considering equation (2), it is possible to write the discrete form of the battery transient equations:

$$\begin{cases} \mathbf{x}_{k+1} = \mathbf{A}\mathbf{x}_k + \mathbf{B}\mathbf{u}_k \\ \mathbf{y}_k = \mathbf{C}\mathbf{x}_k + \mathbf{D}\mathbf{u}_k \end{cases} \quad \begin{cases} \mathbf{u} = [I_t]\mathbf{x} = \begin{bmatrix} U_{RC_1} & U_{RC_2} \end{bmatrix}^T \quad \mathbf{y} = [U_t - U_{OC}] \\ \mathbf{A} = \begin{bmatrix} e^{-t/R_1C_1} & \\ & e^{-t/R_2C_2} \end{bmatrix} \quad \mathbf{B} = \begin{bmatrix} R_1(1-e^{-t/R_1C_1}) \\ R_2(1-e^{-t/R_2C_2}) \end{bmatrix} \\ \mathbf{C} = [1 \quad 1]^T \quad \mathbf{D} = R_0 \end{cases} \tag{5}$$

where R_0, R_1, R_2, C_1 and C_2 are the cell parameters as a function of SOC and thus indirectly varying with time. The vector of state variables **x** is constituted by the two voltages across *R–C* blocks.

As usual, matrix **A** represents the dynamic evolution of state **x**, matrix **B** indicates the quota of input directly transferred to states (algebraic part of *R–C* blocks) and matrices **C** and **D** indicate the influence of state and input into output, constituted by the battery's voltage at its terminals.

The Extended Kalman filter technique is applied to the dynamic system that describes the transient behaviour of the left part of the electrical circuit illustrated in Fig. 5. The EKF uses the measured current (I_t) and the OCV (obtained as the difference between the output of the *R–RC–RC* Network block and the voltage measurements) to perform the runtime SOC evaluation. The detailed equations of this block are as follows:

$$\begin{cases} x_{k+1} = f((x_k, u_k)) + w_k = a_1 x_k + b_1 u_k + w_k \\ y_k = g(x_k) + v_k \\ x = U_{SOC} \\ u_k = I_t \\ y = U_{OC} \\ a_1 = e^{\frac{-t}{R_{sd}C_Q}} \\ b_1 = R_{sd}\left(1 - e^{\frac{-t}{R_{sd}C_Q}}\right) \end{cases} \tag{6}$$

Note that $g(\ )$ is the U_{SOC}–U_{OC} correlation function, that is able to take into account voltage hysteresis, according to the analysis performed in the previous section and summarized by equation (4).

Moreover, w_k and v_k are the process and the measurement noises respectively. They are assumed to be independent to each other and white normal distributions with a zero mean and covariance of known values. Further details about Kalman filter are reported also in Refs. [18,19].

The other difference is that the "mix" block is chosen as a switch that periodically resets the value of *SOC_Ah*: normally is *SOC_ev* = *SOC_Ah*; however periodically it is forced *SOC_ev* = *SOC_kf*, and the integral 1/(Cs) is reset to accommodate for this new output value.

In Section 2.1 it was seen that for high power cells Ampere-hour counting leads to errors on SOC of about 10% after 20 min. Therefore the periodicity of the mix block must be lower than this value. Several simulations were performed on this time, and it was seen that values between 1 and 10 min give the best results.

4. Tests and results

Tests and results are reported in reference to the tests made on the new and on the aged LFP cell. During the tests the SOC evaluation is analysed both for few hours duration and long term stability, that required the SOC evaluation to be extended for tens of hours. For the tests on the standard LFP cell, they are conducted simulating the battery stress on mainly two reference road conventional cycles. After the identification of the cell parameters, the EKF algorithm is applied. The tests are repeated taking as reference the same cycles, after several months, also for the aged cell.

4.1. Test definition

The quality of the SOC estimation applied to the cell is tested on the repetition of two main reference cycles. The two cycles, corresponding to the real usage of the battery on-board hybrid vehicles, are shown in Fig. 12. Currents are negative when the battery is delivering power, positive otherwise. Both of the cycles are scaled at cell level, and a charge compensation is introduced.

The tests are executed by the repletion of several cycles, performing the SOC evaluation through the algorithm.

4.2. Tests on the LFP cell

The test is applied on the LFP cell with reference to the Cycle 1. The cell is subjected to the current profile, then the SOC estimator is applied.

The reference SOC is obtained by numerical integration of current, measured with lab instrumentation, and the parameters of RC network are determined as a function of SOC, then the SOC estimation is performed with the algorithm and finally compared to the measured value. It must also be noted that the proposed algorithm should be able to be implemented onboard real buses, using commercial, inexpensive measuring hardware. To show how the algorithm is able to perform when fed with measures from

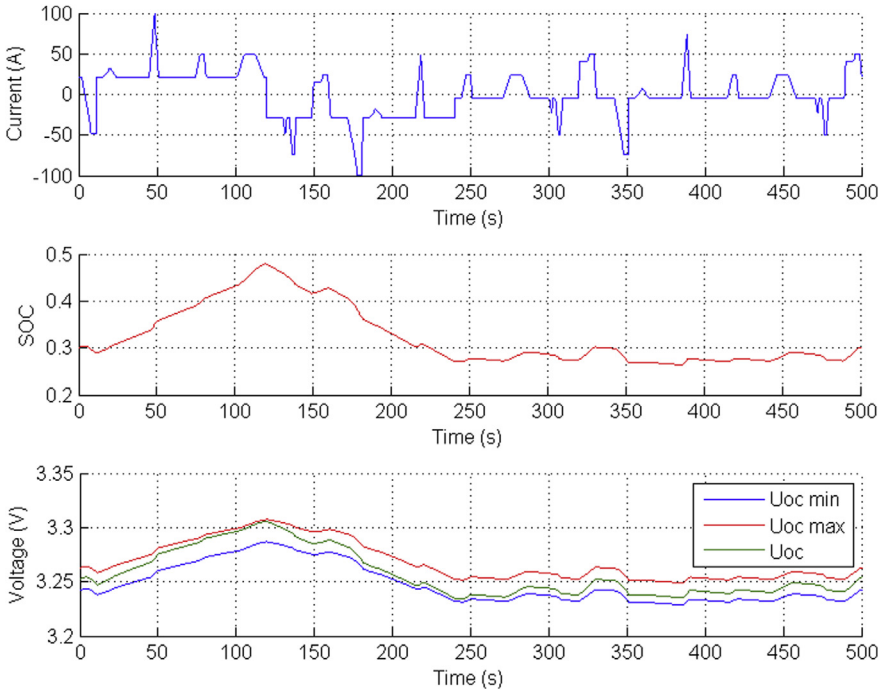

Fig. 9. U_{OC} evaluation with a standardized road current cycle, with superposition of a larger current causing SOC swing.

inexpensive sensors, the voltage and current data supplied to it are altered with respect to the values measured with lab-grade instrumentation as described in equation (7). Current is measured using a shunt, class 0.5 and full scale 150 A; the voltage is measured with a DAQ device (Model NI 9219) with a declared accuracy of 0.3% of reading.

$$\begin{cases} I_{KSE}/A = 1.03 I_{LAB}(t) + 0.2 \\ V_{KSE}/A = 1.02 I_{LAB}(t) + 0.04 \end{cases} \quad (7)$$

i.e., a 200 mA offset and 3% deviation is introduced onto the current, and a 40 mV offset and 2% error is added to the voltage. Moreover the initial SOC is set at 70%, although the real initial SOC of the cell is about 50%. The test lasted 45 h. Fig. 13(a) shows results related to the first part of the test, while some comments about long-term stability are reported later. The estimated SOC by the algorithm (red curve) matches the SOC obtained by the numerical integration of the experimental measured current (blue curve), recovering the initial error in a few hours.

4.3. LFP aged cell: results

After the tests previously described, the cell has one year rest. After this period, Cycle 2 is applied to the aged cell. At first level, to evaluate the stability of the algorithm, no modification for the electrical parameters (R_0, R_1, R_2, C_1, C_2) is applied. At the same, also the EKF w_k and v_k parameters that influence treatment of errors, are kept unmodified. These parameters are normally tuned off-line for each set of electrical parameters (R_0, R_1, R_2, C_1, C_2) related to the specific cell. Finally, also voltage and current errors provided to the experimental data fed to the algorithm present the same trend as described in equation (7).

The test lasts about 45 h and is divided in three parts: a first sequence of 48 cycles, lasting about 5 h, a second phase of rest

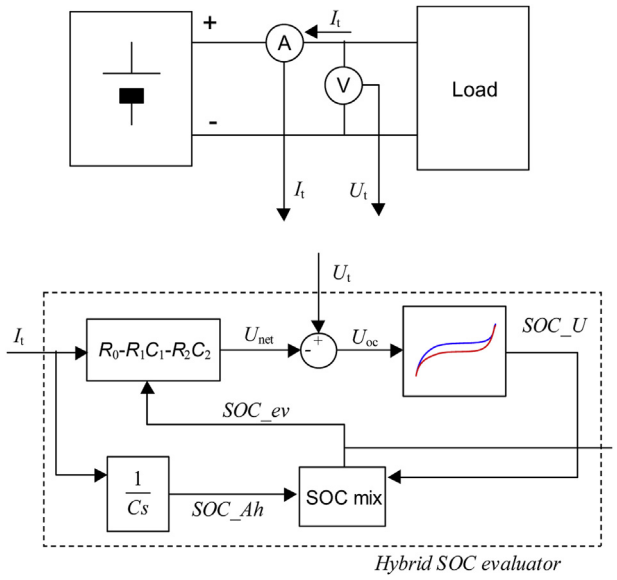

Fig. 10. Hybrid SOC evaluator, basic concept.

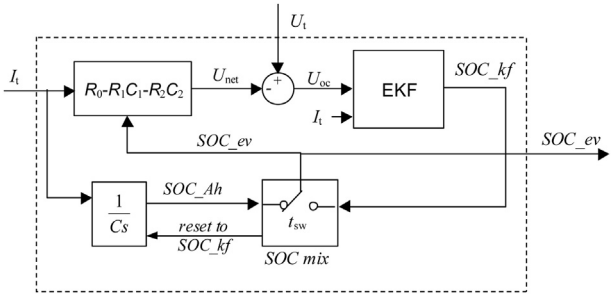

Fig. 11. Hybrid SOC evaluator, actual implementation.

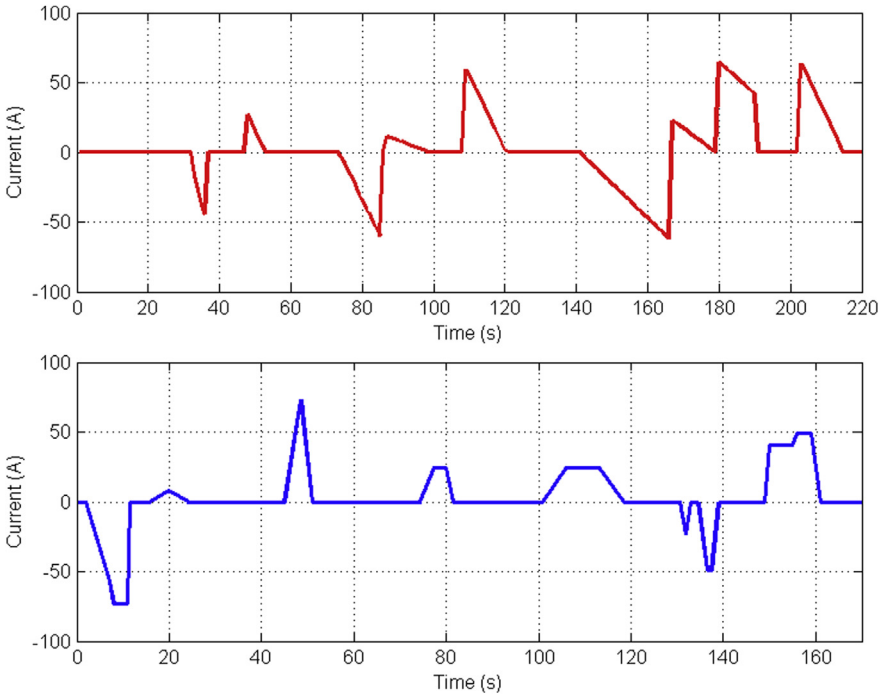

Fig. 12. Cycle 1 (top) and Cycle 2 (bottom) scaled for the battery cell.

(35 h) and the second sequence (5 h). Also for the previous case results are related to the first part of the test, while some comments about long-term stability are reported later. The estimated SOC (red curve) matches the SOC obtained by the numerical integration of the measured current (blue curve) as visible in Fig. 13(b), recovering the initial error in the same time used in the previous test of Fig. 13(a). This aspect is representative of the high level of stability and reliability of the proposed algorithm, able to work properly also without redefinition of the parameters.

The second test is oriented to evaluate the algorithm through a re-calibration of the electrical and the EKF parameters: particularly, a new set of electrical parameters (R_0, R_1, R_2, C_1, C_2) and the

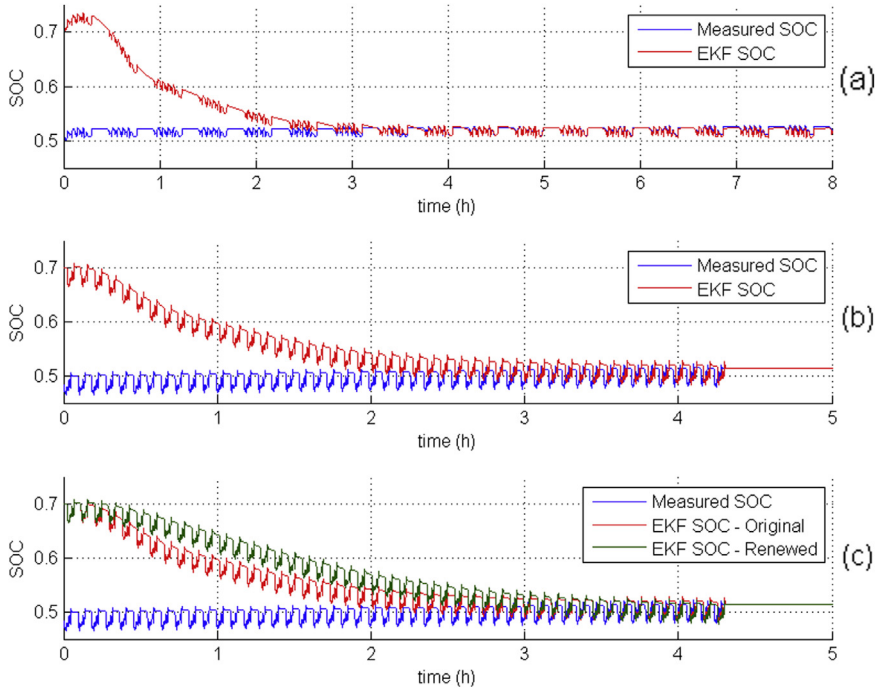

Fig. 13. Experimental evaluation of battery SOC estimation using the EKF-based model for Cycle 1 (a), for Cycle 2 using an aged cell (b), comparison between results obtained both for the aged cell with original (red) and renewed (green) set of electrical and EKF parameters (c). (For interpretation of the references to colour in this figure legend, the reader is referred to the web version of this article.)

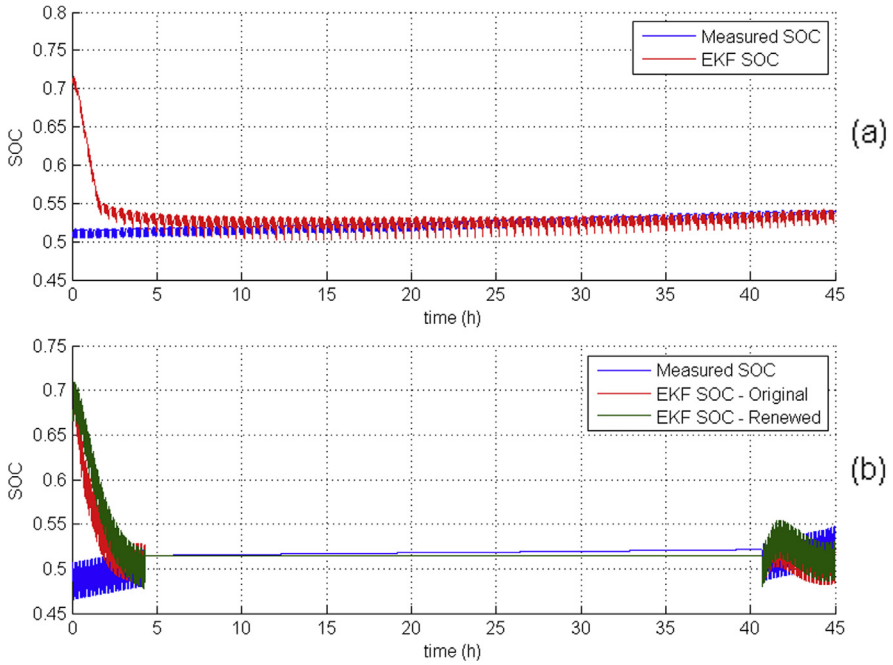

Fig. 14. Experimental validation of the EKF-based model on the Cycle 1 (a), validation of the EKF-based model on the Cycle 2 (b).

SOC–OCV correlation curve are estimated. In this case, providing the same voltage and current errors to the experimental data, the results carried out by the algorithm are less accurate than ones showed in Fig. 13(a). In order to have the same behaviour of the last test SOC, also the EKF parameters w_k and v_k have to be changed. Final result is reported in Fig. 13(c). This aspect shows how the re-calibration of the electrical parameters should be necessarily accompanied with the update of the EKF parameters, to maintain good quality for the SOC estimation. The procedure, fully automatable, can also be performed during the standard vehicle maintenance operations, around once a year.

4.4. Long term stability

The long term stability for the algorithm is analysed in reference to the three case studies already presented above. It is possible to observe that results already mentioned for the LFP cell, subjected to the Cycle 1, show the stability of the algorithm for the total duration of the test, of about 45 h. Results are reported in Fig. 14(a).

Similar results are obtained for the aged cell subjected to Cycle 2 without any electrical or EKF parameters recalibration. It must be also noted that with respect to the previous analysis, the SOC evaluation is stopped during the rest phase of the vehicle: also in this case the stability seems to be guaranteed. Finally, redefining the electrical and the EKF parameters for the aged cell, the evaluated SOC matches the SOC measured through lab instruments more accurately, as reported in Fig. 14(b).

5. Conclusions

This paper has mainly put in evidence the huge difficulties for SOC evaluation of the LFP cell's arising from its characteristics. First of all the high power, that enlarges the accumulation effect of measured errors on the ampere-hour counting. Furthermore, the flat OCV–SOC curve for most practical ranges of SOC, that causes difficulties in evaluating SOC from open-circuit voltage measures, combined with the high level of hysteresis of the OCV–SOC curve correlation.

These difficulties have been dealt at first modelling the voltage hysteresis: transition between charge-based and discharge-based curves has a higher derivative, than the stabilized OCV curves, that eases SOC evaluation. Additionally, an adequate treatment of measurement errors was done using an Enhanced Kalman Filter. The resulting algorithm mixes ampere-hour counting, OCV–SOC evaluation, with an additional correction by a Kalman filter.

The algorithm effectiveness has been evaluated firstly through measures that were taken from lab tests with the highest accuracy. Then the integral of these high accuracy currents was taken as the best estimate of cell's SOC. Finally, the algorithm has been fed with data that were altered so that it was able to simulate measures that could be taken from cheap, industrial sensors. Moreover a wrong initial SOC estimate was supplied to it.

Evaluation was made in several cases, and conditions. In all cases the algorithm recovered the initial errors in reasonable time, and remained stable very near to the "actual" SOC value. The algorithm has also shown "long term stability". Naturally, when the vehicle is at rest, e.g. during nights, it must be made aware of this rest, otherwise it could continuously crunch just measurement errors and offsets, thus leading to unacceptable results. Finally, the algorithm gave good results even after one year of calendar life had passed, which means that no important drift in the cell's behaviour had occurred. However, it is recommended that, when the cells and batteries are used onboard production vehicles, yearly recalibration is made, to keep the algorithm in touch with the actual state of life of cell and battery.

Acknowledgements

The research leading to these results has received funding from the European Union Seventh Framework Programme (FP7/2007-2013) under grant agreement n. 234019 for the Hybrid Commercial Vehicle (HCV) project.

References

[1] Ok Kyung Park, Yonghyun Cho, Sanghan Lee, Ho-Chun Yoo, Hyun-Kon Song, Jaephil Cho, Energy Environ. Sci. 4 (2011) 1621–1633, http://dx.doi.org/10.1039/C0EE00559B.

[2] Massimo Ceraolo, Tarun Huria, Giovanni Pede, Francesco Vellucci, in: IEEE Vehicle Power and Propulsion Conference (VPPC), 2011, 6–9 Sept. 2011, pp. 1–6, http://dx.doi.org/10.1109/VPPC.2011. 6043116.

[3] S. Piller, M. Perrin, A. Jossen, J. Power Sources 96 (2001) 113–120, http://dx.doi.org/10.1016/S0378-7753(01)00560-2.

[4] V. Pop, H.J. Bergveld, P.H.L. Notten, P.P.L. Regtien, Meas. Sci. Technol. 16 (2005) R93–R110, http://dx.doi.org/10.1088/0957-0233/16/12/R01.

[5] Z. Hanlei, C. Mo-Yuen, in: 2010 IEEE Power and Energy Society General Meeting, July 25–29, 2010, pp. 1–6, http://dx.doi.org/10.1109/PES.2010.5590108.

[6] Z. Hanlei, C. Mo-Yuen, in: IECON 2010–36th Annual Conference on IEEE Industrial Electronics Society, Nov. 7–10, 2010, pp. 1844–1849, http://dx.doi.org/10.1109/IECON.2010.5675395.

[7] M. Verbrugge, E. Tate, J. Power Sources 126 (2004) 236–249, http://dx.doi.org/10.1016/j. jpowsour.2003.08.042.

[8] G.L. Plett, J. Power Sources 134 (2004) 252–261.

[9] G.L. Plett, J. Power Sources 134 (2004) 262–276.

[10] G.L. Plett, J. Power Sources 134 (2004) 277–292.

[11] M. Ceraolo, T. Huria, V. Conte, P. Harmut, in: European Electric Vehicle Congress EEVC2012, Brussels, 19–22 November 2012.

[12] Min Chen, G.A. Rincon-Mora, IEEE Trans. Energy Convers. 21 (2) (June 2006) 504–511, http://dx.doi.org/10.1109/TEC.2006.874229.

[13] S.S. Zhang, K. Xu, T.R. Jow, J. Power Sources 115 (1) (27 March 2003) 137–140, http://dx.doi.org/10.1016/S0378-7753(02)00618-3.

[14] G. Nagasubramanian, in: 34th Intersociety Energy Conversion Engineering Conference, 1999, http://dx.doi.org/10.4271/1999-01-2462.

[15] G. Nagasubramanian, J. Appl. Electrochem. 31 (1) (2001) 99–104, http://dx.doi.org/10.1023/A:1004113825283.

[16] Yuriy V. Mikhaylik, James R. Akridge, J. Electrochem. Soc. 150 (2003) A306, http://dx.doi.org/10.1149/1.1545452.

[17] S. Bertoni, M. Ceraolo, T. Huria, in: European Electric Vehicle Congress EEVC2012, Brussels, 19–22 November 2012.

[18] G.L. Plett, J. Power Sources 134 (2004) 252–292.

[19] Z. Chen, Y. Fu, C. Mi, IEEE Trans. Veh. Technol. 62 (3).